Chemical Engineering Journal 347 (2018) 618–630

Contents lists available at ScienceDirect

Chemical Engineering Journal

journal homepage: www.elsevier.com/locate/cej

Phosphate recovery from real fresh urine by $Ca(OH)_2$ treated natural zeolite

Dimitris Mitrogiannis[a,*], Maria Psychoyou[a], Nikolaos Koukouzas[b], Nikolaos Tsoukalas[b], Dimitrios Palles[c], Efstratios Kamitsos[c], Avgoustos Pantazidis[a], Georgios Oikonomou[d], Ioannis Baziotis[a]

[a] Department of Natural Resources Management and Agricultural Engineering, Agricultural University of Athens, 75 Iera Odos, 11855 Athens, Greece
[b] Centre for Research and Technology Hellas (CERTH), Chemical Process and Energy Resources Institute (CPERI), 52 Egialias str., 15125 Maroussi-Athens, Greece
[c] Theoretical and Physical Chemistry Institute, National Hellenic Research Foundation, 48 Vassileos Constantinou Avenue, Athens 11635, Greece
[d] Institute of Geology and Mineral Exploration, Olympic Village Acharnae, Athens 13677 Greece

HIGHLIGHTS

- Zeolite treated with $Ca(OH)_2$ adsorbed phosphate P from real fresh urine.
- Total P removal was due to adsorption and liquid phase precipitation.
- Modified zeolite exhibited a higher P adsorption capacity than natural zeolite.
- More P adsorbed onto CaT-Z surface than precipitated in the liquid phase.
- Fresh urine dilution affected the adsorbed P speciation.

GRAPHICAL ABSTRACT

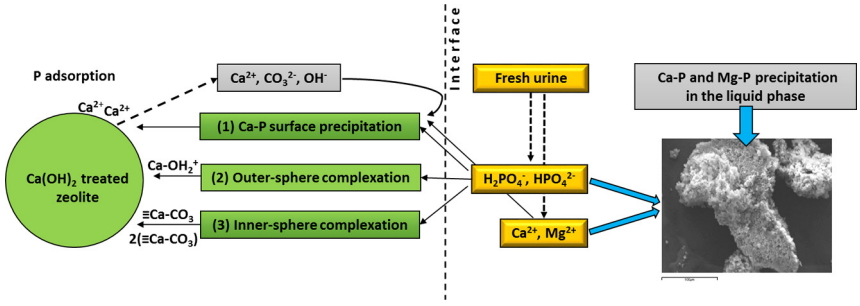

ARTICLE INFO

Keywords:
Human urine
Zeolite
Phosphate recovery
Precipitation
Ligand exchange

ABSTRACT

Source-separation of urine can provide an alternative way for wastewater treatment and nutrients recovery by adsorbents which then can be applied in the agriculture as fertilizer. In this work, natural (NZ) and $Ca(OH)_2$ treated zeolite (CaT-Z) were employed in batch tests for adsorption of phosphate phosphorus (P) from real fresh urine (FU). Total P removal was a simultaneous process of adsorption on NZ or CaT-Z surface and precipitation in the liquid phase as Ca-P and Mg-P containing precipitates. In the presence of CaT-Z, the contribution of adsorption on total P removal was higher than that of the liquid phase precipitation at all dilution ratios of FU with deionized water. Lower residual P concentrations in FU and more P bound on the adsorbent were observed for CaT-Z than for NZ. The sequential desorption study showed that 55.1–84.9% and 6.2–72.6% of total removed P was recovered from FU loaded CaT-Z and NZ, respectively. In less diluted FU, CaT-Z adsorbed much more P (up to 11.11 mg/g) than NZ due to the dominant contribution of inner-sphere complexation (ligand exchange). In more diluted FU, outer-sphere complexation was the major P adsorption mechanism accompanied by ligand exchange. Phosphorus removal by CaT-Z reached an equilibrium in 72–96 h. Bulk (XRD, IR-ATR) and in-situ (EPMA, SEM-EDS) analytical techniques clarified the adsorption mechanisms and confirmed the accommodation of Ca-P phases on NZ and CaT-Z. The results of the study suggested the suitable use of CaT-Z for simultaneous PO_4-P and NH_4-N recovery from human urine.

* Corresponding author.
E-mail address: mitrogdimi@gmail.com (D. Mitrogiannis).

https://doi.org/10.1016/j.cej.2018.04.102
Received 13 December 2017; Received in revised form 19 March 2018; Accepted 16 April 2018
Available online 17 April 2018

1. Introduction

The sustainable approach of an effective wastewater treatment takes account of both the removal of pollutants and recovery of valuable components [1]. Nitrogen (N) and phosphorus (P) are essential nutrients for plant production but their presence in effluents obtained from various human activities can cause eutrophication of surface water bodies. Human urine is a wastewater with high loads of nutrients (N, P and K), although it contributes to less than 1% of the total domestic wastewater volume [1,2]. Urine can be converted from a wastewater stream to a sustainable source of valuable nutrients for crop fertilization by recovering them. According to estimates [3], phosphate P recovered from urine could satisfy a significant percentage (22%) of the global P demand. Alternative P sources are important considering the scenarios of the quantitative and qualitative depletion of non-renewable P resources (phosphate rock reserves) in the next decades and the increasing prices of phosphate fertilizers due to rising costs in mineral extraction and processing [4]. Source separation of urine is a future trend through the use of no-mix toilets and waterless urinals which have been already introduced in developing and developed countries [2,5–7]. Urine separation can improve the effluent quality as well as the capacity and function of existing municipal wastewater treatment plants by reducing their energy consumption and scaling of struvite in pipe walls. To reduce the transport costs in central plants, source-separated urine could be treated in decentralized scale (e.g. big buildings, public places) by using simpler and low-tech treatment methods available in local communities [2,8].

Physical, chemical, biological and combined methods have been proposed for the removal or recovery of nutrients from “yellow water” (human urine) such as ammonia stripping, evaporation, reverse osmosis, microalgae cultivation, anion exchange, adsorption, struvite and calcium phosphate precipitation [9–15]. Regarding P, biological removal and chemical precipitation have their limitations such as ammonia toxicity to microalgae cultivated in undiluted urine, high input of chemical reagents or low phosphate selectivity in diluted urine during precipitation [12,16]. For struvite crystallization, up to 75–90% of the operational costs are due to the required addition of alkaline reagents (NaOH) and Mg^{2+} salts [1].

On the other hand, there are risks or disadvantages by the direct use of human urine as fertilizer due to transport, storage, smell and hygiene issues (presence of pathogens, pharmaceuticals and hormones) [10,17]. Another important issue is the potential negative effect of urine salinity on plants. For these reasons, the selective adsorption of nutrients from urine on eco-friendly materials presents advantages for crop fertilization, keeping low risk to public health. Adsorption process is considered as an efficient, simple and low-cost method for PO_4-P removal even at low P concentrations [18,19]. Nutrient loaded clinoptilolite obtained after treatment of diluted urine solutions has been used as a fertilizer resulting in higher biomass productivity of mixed grass than the direct application of undiluted and diluted urine [17].

Most studies, using natural zeolites (NZ) for human urine treatment, have been focused on ammonium adsorption [6,10,20–22]. A limited number of researches has examined the P adsorption from urine by minerals such as raw clinoptilolite [6,17,23] and natural loess [24], whereas hybrid anion exchange resins [11,25,26] and zirconium-based metal-organic framework [27] have been also used in synthetic urine. Among these P adsorption works, only a few were conducted in real human urine, either in real hydrolysed (HU) [24] or in real fresh urine (FU) [6,23]; the latter two used however raw NZ (for NH_4^+ adsorption) in combination with MgO (for struvite precipitation) without getting insight into adsorption mechanisms. Therefore, there is a literature gap regarding P adsorption studies in real fresh urine. Our previous work showed that $Ca(OH)_2$ treated natural zeolite (CaT-Z) efficiently adsorbed phosphate anions from aqueous solutions focusing on low initial P concentrations typical for effluents of municipal wastewater treatment [28].

In the present study, CaT-Z is used for the first time in real wastewater (WW) treatment, where P adsorption on the solid matrix and precipitation in the liquid phase can simultaneously take place during a batch process [29–31]. Recent studies have shown that even raw NZ (clinoptilolite) can remove P from high-strength real WW due to assistance of ammonium adsorption on zeolite which consequently promoted Ca-P precipitation [30,31]. In contrast, the P adsorption on NZ was very low in pure P aqueous solutions with similar concentrations of WW [28,30]. So, it is important to investigate whether CaT-Z can adsorb more P than NZ in real WW without being dependent on the alkaline WW pH or on ammonium concentration and adsorption. Additionally, it would be useful for the design and evaluation of recovery process to quantify and distinguish the contribution of adsorption from that of liquid phase precipitation to the total P removal [29]. This issue has not been extensively investigated in recent studies [30,31].To the best of our knowledge, it is the first time that real FU is used for P recovery only through adsorption. An advantage of FU treatment is the direct nutrient recovery at the beginning of collection system and in a shorter storage time than that needed for HU (at least 6 months). Moreover, more P could be potentially adsorbed from FU on the solid phase before its spontaneous precipitation during storage [26], making its separation easier by sieving a relatively coarser loaded adsorbent. Batch tests were performed in two series by using two different samples of fresh urine (FU-1 and FU-2). The chemical composition of FU varies with person, diet and day time [5], and it changes during storage due to various spontaneous processes such as urea hydrolysis, ammonia loss through volatilization and phosphate precipitation with Ca^{2+} and Mg^{2+} ions [7,11].

As main objective of this work, the first experimental series aimed to compare NZ and CaT-Z as P adsorbents in FU-1 without adjustment of original pH. This series started the day after FU-1 collection, lasted two weeks and investigated the effect of contact time and urine dilution on P removal as well as the adsorption mechanisms. The second experimental series was conducted with a newly collected urine sample (FU-2) by using only CaT-Z, since it was proved more efficient than NZ in the first series and in order to minimize changes in FU-1 chemical composition during storage longer than two weeks. The goal of the second experimental series with FU-2, completed within two weeks after collection, was to compare P adsorption/recovery under varied FU compositions and to examine the effect of more operational parameters (contact time, urine dilution, urine pH and temperature). A range of spectroscopic and in-situ techniques – X-ray diffraction (XRD), Scanning Electron Microscopy-Energy Dispersive System (SEM-EDS), Electron Probe Micro-analyzer (EPMA) and Infrared Attenuated Total Reflectance (IR-ATR) – were used to characterize the adsorbents and to clarify the adsorption mechanisms. Finally, we applied a sequential desorption procedure in order to estimate the contribution of liquid phase P precipitation on the total P removal and to further study the P adsorption mechanisms.

2. Materials and methods

2.1. Adsorbent pretreatment

The preparation of raw natural zeolite and its pretreatment process with solution of 0.25 mol/L $Ca(OH)_2$ are described in our previous work [28]. In the present study, the raw mineral was sieved to particle size of 0.5–1.19 mm.

2.2. Collection of urine sample

Two different FU samples (FU-1 and FU-2) were collected within 24 h from a forty year old male working in Agricultural University of Athens. Each sample (ca. 1.5 L volume) was collected on different day and stored in a plastic bottle at 4 °C. The day after collection the basic physicochemical properties of FU samples were determined (Table 1).

Table 1
Physicochemical properties of real undiluted fresh urine (FU-1 and FU-2) used in batch adsorption tests (SD: standard deviation, n = 3).

	FU-1	FU-2
Parameter	Mean ± SD	Mean ± SD
pH	5.80 ± 0.06	5.67 ± 0.01
EC (mS/cm)	9.68 ± 0.19	14.77 ± 0.16
PO_4-P (mg/L)	400.0 ± 8.4	670.9 ± 7.6
NH_4-N (mg/L)	492.8 ± 16.6	401.7 ± 15.1
Na^+ (mg/L)	1341.7 ± 52.0	1852.6 ± 48.2
K^+ (mg/L)	562.5 ± 21.7	2325.0 ± 106.1
Ca^{2+} (mg/L)	587.8 ± 79.9	936.3 ± 109.7
Mg^{2+} (mg/L)	41.5 ± 2.4	18.4 ± 0.4

The FU-1 solution was characterized by a lower P concentration and ionic strength (EC) than the ones of FU-2 solution. Both FU-1 and FU-2 contained high calcium concentration compared with the typical values mentioned in the literature [7], whereas the rest properties values were within the reported ranges. Urine also contains high amounts of total dissolved solids and various substances such as sulfate, chloride and organic macromolecules which were not measured in this study.

2.3. Adsorption experiments

All adsorption experiments were conducted in batch mode at a constant adsorbent dosage of 10 g/L. Twenty mL of fresh urine (FU-1 or FU-2) were added in a 30 mL bottle of high-density polyethylene (HDPE) which contained 200 mg adsorbent. The bottles were capped and shaken at 200 rpm with a horizontal shaker which was placed in a temperature-controlled chamber. The tests were performed in triplicate and the average values of measured parameters are reported.

To exclude precipitates and suspended solids from the working solution, undiluted fresh urine was filtered with filter paper (MN 615, Macherey-Nagel, Germany) prior to each batch test. For more accurate results on the calculation of P removal efficiency and adsorption capacity, the initial P concentration (C_o) was measured at each dilution ratio of FU before adding the adsorbent (Table 2). Phosphate P and ammonium N concentrations in FU were expressed as mg P/L and mg N/L, respectively. After adsorption, samples were collected from the supernatant with a plastic syringe, filtered through 0.45 μm polyester syringe filters (Chromafil PET, Macherey-Nagel, Germany) and placed in Eppendorf type centrifuge tubes (1.5 mL). The samples were analyzed within 24 h for N, P, Na and K content. Calcium and magnesium concentrations were determined after a few days from acidified samples stored at 4 °C.

The kinetic experiments were performed at 25 °C by using 500 mg adsorbent and 50 mL of FU-1 or FU-2 at 50/50 dilution ratio with DI (V_{DI}/V_{urine}) which were contained in HDPE bottles of 100 mL capacity (Table 2). The kinetic test with FU-1 was conducted by using NZ, CaT-Z and control samples with no adsorbent. Samples (50 μL) of FU-1 were withdrawn from the supernatant with a micropipette at different time intervals: 1, 4, 24, 48, 72, 96, 120 and 144 h. In the kinetic test with FU-2 and CaT-Z, additional samples were collected at 2, 3 and 8 h. At the same time, a kinetic test was run with control samples consisted of FU-2 with no CaT-Z. Prior to P analysis, the samples of both kinetic tests were diluted with DI and centrifuged for 5 min at 4000 rpm.

Equilibrium tests with FU-1 and FU-2 were conducted for 144 h at five dilution ratios of FU with DI (V_{DI}/V_{urine}: 25/75, 50/50, 75/25, 90/10 and 95/5). These ratios correspond to 75%, 50%, 25%, 10% and 5% FU solution [$100 \times V_{urine}/(V_{urine} + V_{DI})$], respectively (Table 2). The initial pH of each dilution ratio was not chemically adjusted since the dilution resulted in a slight increase of pH by 0.1–0.15 units due to the buffering capacity of fresh urine. The equilibrium tests with FU-1 were performed at 25 °C by using NZ and CaT-Z, whereas the tests with FU-2 and CaT-Z were run at the same time at 25 and 35 °C using two different temperature-controlled chambers in order to examine the effect of FU-2 temperature on P removal.

The influence of fresh urine pH on P removal by CaT-Z was examined at 25 °C and in 50% FU-2. The initial pH of FU-2 was adjusted to the desired values (5, 6, 7 and 8) using HCl and/or NaOH before adding the adsorbent. The final solution pH was measured after 144 h. The adsorption capacity of NZ and CaT-Z for P at equilibrium, q_e (mg/g), and the P removal efficiency ($R\%$) were calculated by the Eqs. (1) and (2), respectively. It should be noted that $R\%$ could include both P precipitation in the liquid phase and adsorption on the solid phase.

$$q_e = (C_0 - C_e)V/m \quad (1)$$

$$R\% = 100 \times (C_0 - C_e)/C_0 \quad (2)$$

where C_o *and* C_e are the initial P concentration and concentration at equilibrium (mg/L), respectively, V is the volume of the urine solution (L) and m is the adsorbent mass (g).

2.4. Desorption tests

A sequential extraction procedure of three steps (0.5 M $NaHCO_3$ at pH 8.5, 0.1 M NaOH and 0.5 M HCl) [32,33] was applied to the loaded NZ and CaT-Z in order to determine the P fractionation and to estimate the contribution of liquid phase precipitation on the total P removal (R %). The desorption study was run in triplicate at 200 rpm and 25 °C by using 10 mL of eluent and 100 mg of FU-1 loaded NZ and CaT-Z obtained after the isotherm experiment at 25 °C and at 25/75, 50/50, 10/

Table 2
Experimental conditions of P removal from fresh urine (FU-1 and FU-2) by NZ and CaT-Z (contact time = 144 h, adsorbent dosage = 10 g/L).

Variable	Solution	Adsorbent	Dilution ratio (V_{DI}/V_{urine})	%FU*	C_0 (mg P/L)	pH	T (°C)
Contact time	FU-1	NZ, CaT-Z	50/50	50	189.5 ± 11.7	5.80	25
Urine dilution	FU-1	NZ, CaT-Z	25/75	75	306.4 ± 7.9	5.80	25
			50/50	50	200.0 ± 4.2		
			75/25	25	103.0 ± 6.4		
			90/10	10	39.9 ± 3.4		
			95/5	5	20.0 ± 0.3		
Contact time	FU-2	CaT-Z	50/50	50	320.7 ± 6.1	5.67	25
Initial pH	FU-2	CaT-Z	50/50	50	394.8 ± 6.6	5–8	25
Urine dilution	FU-2	CaT-Z	25/75	75	505.0 ± 22.9	5.67	25, 35
			50/50	50	335.4 ± 3.8		
			75/25	25	163.3 ± 1.1		
			90/10	10	59.6 ± 1.7		
			95/5	5	29.4 ± 0.4		

* $\%FU = 100 \times V_{urine}/(V_{DI} + V_{urine})$.

Table 3
EDS qualitative results of precipitates collected after treatment of 50% FU-1 with NZ and CaT-Z (C_0 = 200.0 mg P/L, pH = 5.8, adsorbent dosage = 10 g/L, contact time = 144 h, T = 25 °C).

Adsorbent	EDS probe location[a]	Ca	P	K	Mg	Na	Cl	S
NZ	1	++[b]	+			+++	+++	
	2	++	++	++	+	+	++	+
	1	+++	+++	+	+	++	+++	+
CaT-Z	1	+++	+++		+			
	1	+++	++					
	1	+++	+++					
	1	+++	+++					

[a] 1: single point analysis; 2: area analysis.
[b] +, ++, and +++: low, medium and high level of the relative intensity for each element, respectively.

90 and 5/95 dilution ratio. After each extraction step (24 h) the adsorbents were washed four times with DI and then dried overnight. The same sequential desorption procedure was conducted with 25% and 5% FU-2 loaded CaT-Z obtained after the isotherm test at 25 °C. The desorption efficiency ($D\%$) and capacity (q_{des}; mg P/g) of each eluent for P were calculated according to the following equations:

$$D\ (\%) = 100 \times (C_{des}/C_{ads}) \quad (3)$$

$$q_{des} = C_{des} V/m \quad (4)$$

where $C_{ads} = (C_0 - C_e)$ and C_{des} are the P concentration (mg/L) in the adsorbent phase and desorption solution, respectively, V is the eluent volume (L) and m is the loaded NZ or CaT-Z mass (g).

To determine the presence of NH_4-N on the adsorbent surface, FU-1 loaded NZ and CaT-Z were extracted for 24 h with 1 M NaCl [34] at a adsorbent/eluent ratio of 50 mg/5 mL. For this desorption series, NZ and CaT-Z samples obtained from the isotherm test at 25 °C and at the above mentioned four dilution ratios of FU-1 were used. The NH_4-N desorption capacity (mg N/g) was calculated according to the Eq. (4).

2.5. Analytical methods

The PO_4-P and NH_4-N concentration in FU was measured following the ascorbic acid (4500-P) and phenate (4500-NH_3) colorimetric standard methods at 880 and 640 nm [35], respectively, by using a UV–vis spectrophotometer (Hach-Lange DR 2800, Germany). The concentration of K^+ and Na^+ was determined by flame photometer (BWB XP, UK) whereas those of Ca^{2+} and Mg^{2+} by atomic absorption spectrometer (Spectra AA10, Varian). Electrical conductivity (EC) and pH values were measured with a portable calibrated conductivity meter (Consort C931, Belgium) and a pH-meter (Metrohm 827, Swiss), respectively.

Samples of NZ and CaT-Z were examined before and after the adsorption tests for their texture, in-situ major elements, mineral mode and functional groups, using the SEM-EDS, XRD and IR-ATR techniques, as described in our previous work [28]. The SEM-EDS was also used to examine precipitated particles collected from 50% FU-1 through centrifugation after the treatment with NZ and CaT-Z. Additionally, major element compositions of the constituent minerals were determined in polished mounted grains in resin using JEOL JXA-8900 Superprobe equipped with four wavelength-dispersive spectrometers (WDS) and one Energy Dispersive Spectrometer (EDS) at the laboratory of Mineralogy and Geology, Agricultural University of Athens. All analyses used 15 kV accelerating voltage, 15nA beam 5 μm wide, 20 s on-peak counting time and 10 s for each background. Natural minerals standards used were quartz (Si), ilmenite (Ti, Mn), corundum (Al), fayalite (Fe), olivine (Mg, Ni), diopside (Ca), microcline (K), jadeite (Na), apatite (P), and chromite (Cr). Further, X-ray maps were collected from selected areas at 15 kV, 15nA, 0.5 μm step size, and 150 ms dwell time giving collection times between 2 and 5 h. X-ray maps for different elements are given in order to inspect the spatial distribution and accommodation of phosphorus in zeolite.

The specific surface area, the total pore volume and the pore average size of NZ and CaT-Z were measured by the Brunauer-Emmett-Teller (BET) method based on the N_2 gas adsorption/desorption isotherms at 77 K and relative pressure (P/P_0) range of 0.0048–0.9915 using a surface area and porosity analyzer (TriStar 3000, Micromeritics). Before N_2 adsorption, the samples of NZ and CaT-Z were outgassed under vacuum at 250 °C for 18 h. The analysis was conducted at the Centre of Research and Technology Hellas (Thessaloniki, Greece).

3. Results and discussion

3.1. Characterization of adsorbents

3.1.1. SEM-EDS analysis

The presence of P on the loaded NZ and CaT-Z was confirmed by the qualitative elemental analysis of EDS (Supplementary material, Fig. S1A–C, spectra #1-3). In the EDS spectra of loaded CaT-Z (#2-3), the P peaks were associated with Ca ones of higher relative intensity than these of loaded NZ (spectrum #1). The SEM images of loaded NZ and CaT-Z showed that the presence of Ca-P phases was associated with the mineral clinoptilolite (Fig. S1A–C).

The precipitates, collected from FU-1 treated with NZ and CaT-Z, consisted of crystals with heterogeneous shape (Fig. S1D–E) and were characterized by different chemical compositions (Fig. S1, spectra #4-5). According to the EDS qualitative analysis (Table 3), the precipitates collected from FU-1 after treatment with NZ contained various elements such as Ca, P, Mg, Na, S and Cl (and minor – close to detection limit – K) which are abundant in human urine. On the other hand, only three elements (Ca, P and Mg) were detected on the precipitates collected from FU-1 in the presence of CaT-Z, mainly consisted of Ca and P, suggesting the calcium phosphate as the dominant phase. The major difference between the two types of precipitates is the NaCl-bearing in the case of treatment with NZ, which is totally absent in CaT-Z. A possible explanation is that NZ still contains energetically sodium-rich sites on its surface, able to be exchanged by solution cations and react with the Cl^- of FU. In contrast, in the CaT-Z, Na^+ has been replaced with Ca^{2+}, therefore, Cl^- may remain in FU, prohibiting the NaCl saturation and precipitation.

3.1.2. EPMA and X-ray maps

The EPMA showed that NZ and CaT-Z revealed rough and heterogeneous surface which consists of zeolite and igneous relics like plagioclase and K-feldspar (Figs. 1–3). Plagioclase is present as anhedral grains in the fragments of CaT-Z sample (Fig. 1A); adjacent to the plagioclase, a zeolite bearing (clinoptilolite) area occurs showing lower relief and flowing texture (probably inherited from the igneous precursor) (Fig. 1B and D). The chemical composition of clinoptilolite ($Si^{4+}/(Al^{3+} + Fe^{2+}) > 4$) ranges for SiO_2 (64.8–69.7 wt%), Al_2O_3 (12.2–13.0 wt%), FeO (0.01–0.11 wt%), MgO (0.92–0.99), CaO (2.26–2.53 wt%) and K_2O (1.49–2.26 wt%) (Table S1).

The chemical analysis of the FU-1 loaded NZ and Ca-T samples showed different zeolite compositions than the CaT-Z samples before adsorption (Table S1). In FU-1 loaded NZ, silicate minerals such as quartz (Qtz), plagioclase (Pl) and potassium feldspar (K-Fsp) were determined (Fig. 2A). The alternated groundmass was also found to be a zeolite enriched area (Fig. 2C). The presence of apatite or other Ca-P phases in plagioclase surface confirmed the P adsorption from FU-1 on NZ (Fig. 2B), as shown by a P_2O_5 percentage of 0.32% in the single point analysis #4 (Table S1). In FU-1 loaded CaT-Z, groundmass is the most alternated (Fig. 3A–D) and the P is adsorbed on the zeolite with a percentage of 0.8–1.06% according to P_2O_5 in analyses #6 (Table S1)

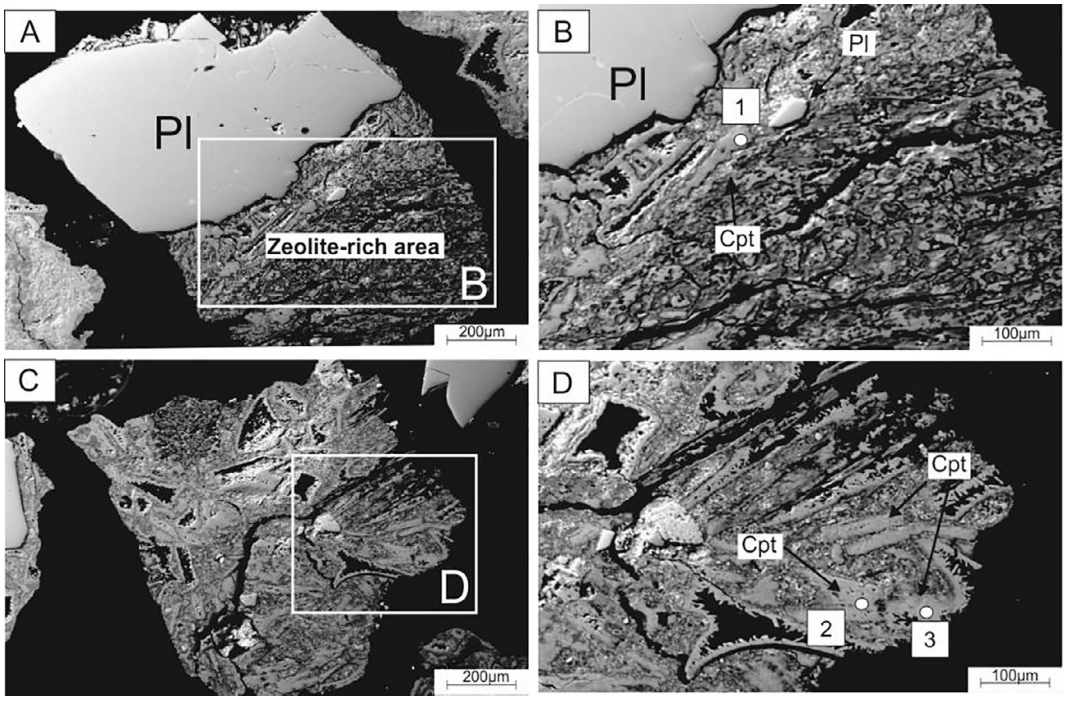

Fig. 1. Silicate minerals inherited from the volcanic precursor and alterated groundmass in two polished – mounted on resin – grains (A, C) of CaT-Z before adsorption. The Cpt is represented as microprismatic fine-grained crystals within the matrix (B, D). Mineral abbreviations: Cpt: clinoptilolite, and Pl: plagioclase. Numbers 1–3 correspond to in-situ EPMA analysis given in Table S1.

and #7 (Fig. 3B, Table S1), respectively.

X-ray maps applied on three different areas of loaded adsorbents (one for NZ and two for CaT-Z) have been examined for the elements Mg, Ca, P, K and Si (Fig. 4 and S2; Fe map is excluded because of the low counts). The close inspection of the zeolite-rich areas suggests that Mg and Si are homogeneously distributed even at higher resolution (Panel A, Fig. S2). The even distribution of Mg and Si suggests that these elements were largely unaffected during zeolite treatment (Panel B in Fig. S2 and C in Fig. 4). Further, the P-rich areas are correlated with the Ca content, while uncorrelated with K. Hence, P and Ca are mainly sequestered at the subgrain boundaries or alternatively at the areas where the fluid was easier to infiltrate the host rock. The former suggests the formation of Ca-P phases and verified the individual EPMA analysis (Table S1).

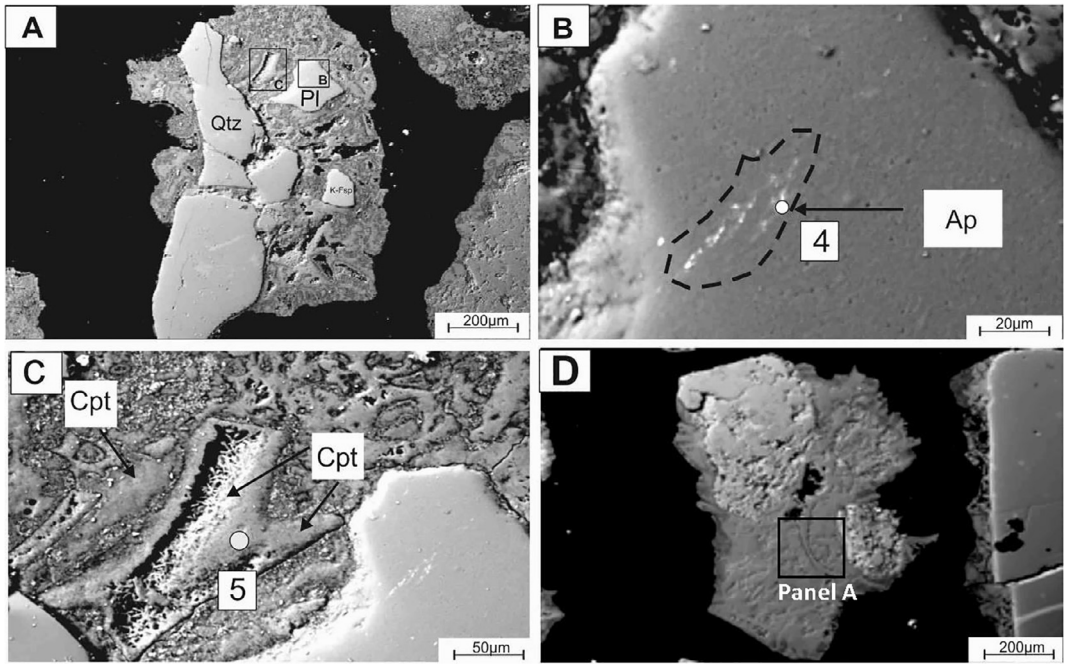

Fig. 2. Quartz, plagioclase and K-feldspar coexist in an alterated matrix (A, C, D) of the loaded NZ in 50% FU-1. Apatite inclusion, within the plagioclase, is shown as oriented micro-crystals (B). The Cpt is formed at the expense of the plagioclase host as suggested by the eroded rims (C). Mineral abbreviations: Qtz: quartz, K-Fsp: potassium feldspar, and Ap: apatite. Numbers 4–5 correspond to in-situ EPMA analysis given in Table S1. Rectangle featured as "Panel A" corresponds to X-ray map area given in Fig. S2.

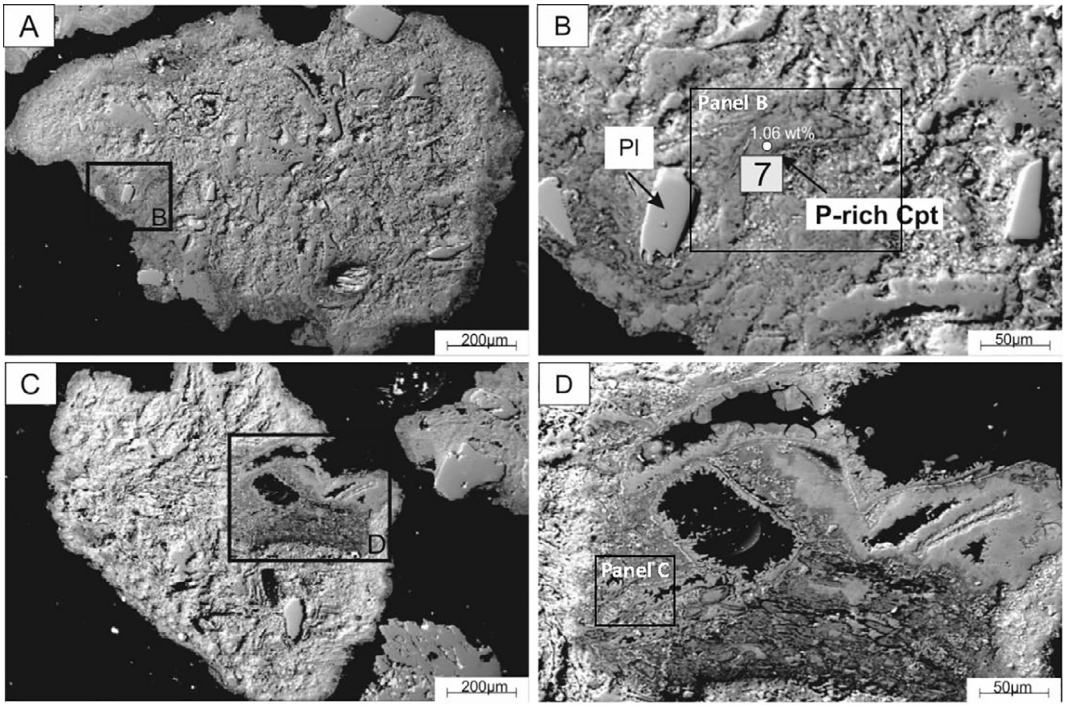

Fig. 3. Polished – mounted on resin – grains of loaded CaT-Z in 50% FU-1 (A, C); Phosphorus-rich areas within the Cpt dominated matrix (B, D). Number 7 corresponds to in-situ EPMA analysis given in Table S1. Rectangles featured as "Panel B" and "C" correspond to X-ray map areas given in Fig. S2 and Fig. 4, respectively.

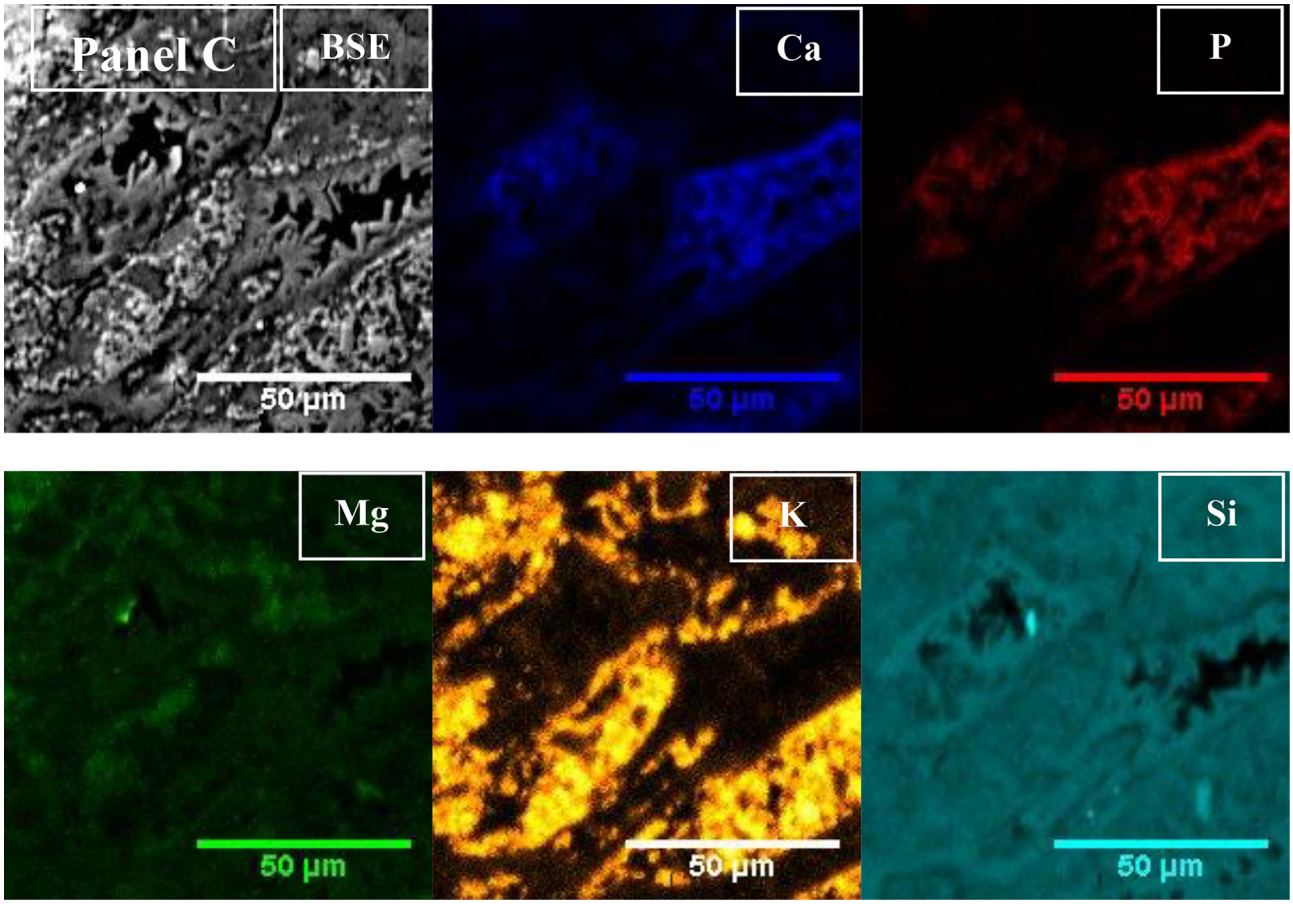

Fig. 4. Panels of qualitative X-ray maps of the zeolite-rich areas featured in Fig. 3 for CaT-Z (Panel C) in 50% FU-1. Brighter color-scale values in the X-ray maps indicate higher concentration of the indicated elements. BSE: backscattered electron images.

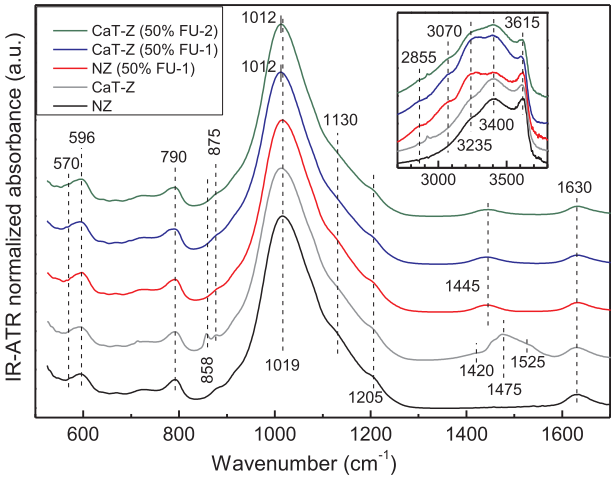

Fig. 5. IR-ATR spectra of the NZ (black line), CaT-Z (grey line), loaded NZ and CaT-Z in 50% FU-1 (red and blue line, respectively), and loaded CaT-Z in 50% FU-2 (green line). For the inset the spectra were normalized with respect to the water H-O-H bending vibration intensity at 1630 cm^{-1}. (For interpretation of the references to color in this figure legend, the reader is referred to the web version of this article.)

3.1.3. XRD analysis

The XRD pattern of NZ showed the presence of clinoptilolite, quartz, anorthite (plagioclase), illite and montmorillonite (Fig. S3a). The same mineral phases, along with K-feldspar, were detected in the XRD pattern of CaT-Z except for montmorillonite (Fig. S3b). In loaded NZ and CaT-Z obtained from 50% FU-1 (Fig. S3c and d), the phases of clinoptilolite, quartz, anorthite, illite and K-feldspar were detected. The only P-bearing mineral phase, berlinite ($AlPO_4$), was revealed in the loaded samples of NZ (Fig. S3c) and CaT-Z (Fig. S3e) in 50% FU-1 and FU-2, respectively. Berlinite was not detected in our previous work [28]. No calcium phosphate phase was detected in the loaded NZ or CaT-Z neither in FU-1 nor in FU-2 solution, although Ca-P phases were confirmed by SEM-EDS (Fig. S1) and EPMA analyses (Figs. 1–4). This indicates that P was adsorbed either as amorphous Ca-P phase or as apatite, however, at a modal content below the threshold number of the applied technique (XRD).

3.1.4. IR-ATR analysis

The functional groups in the IR-ATR spectra of the NZ and CaT-Z before adsorption (Fig. 5) are described in our previous work [28]. The IR spectra of the FU-loaded NZ and CaT-Z samples are similar to each other (Fig. 5). First, they all show the absence of the broad 1400–1580 cm^{-1} envelope assigned to the asymmetric stretch (v_3) of CO_3^{2-} anions. Second, the narrow peaks at 858 and 875 cm^{-1} of CaT-Z, which can be assigned to the out-of-plane bend (v_2) of the carbonate anions (CO_3^{2-}) in aragonite and calcite, respectively, are not present any more in the spectra of the loaded CaT-Z samples (in FU-1 and FU-2). Third, all spectra show a new feature at ca. 1445 cm^{-1} and shoulders developing at ca. 2855 and 3070 cm^{-1} (inset of Fig. 5). The disappearance of the 1400–1580 cm^{-1} envelope and of the 858 and 875 cm^{-1} features from the spectra of loaded CaT-Z samples is most likely due to a ligand exchange reaction between the CO_3^{2-} of CaT-Z and PO_4^{3-} anions of FU [28,36].

The infrared response of PO_4^{3-} anions is expected to be dominated by the triply degenerate IR active modes due to the asymmetric stretch $v_3(PO_4^{3-})$ and bend $v_4(PO_4^{3-})$ vibration of the orthophosphate anions. The frequency and shape of the corresponding infrared bands depend on the charge-balancing cation and deviations from the tetrahedral symmetry. For example, $v_3(PO_4^{3-})$ was measured as a single band at 960 cm^{-1} for Ag_3PO_4 [37] and at 1006 cm^{-1} for $MgNH_4PO_4{\cdot}6H_2O$ (struvite, a biomineral present in human urine sediments) [38] or as a three-component band with contributions at 980, 1008 and 1075 cm^{-1} for Cu-molybdo-phosphate glasses [39]. Likewise, the corresponding $v_4(PO_4^{3-})$ mode was measured in the infrared spectrum at 552 cm^{-1} [37], 571 cm^{-1} [38] and as three components at 560, 605 and 650 cm^{-1} [40]. The presence of the broad and strong NZ silicate band (Si-O-Si asymmetric stretching vibrations) at ca. 1019 cm^{-1} (Fig. 5), in combination with the low phosphorus content of the FU-loaded NZ and CaT-Z samples (Table S1), suggest that no separate $v_3(PO_4^{3-})$ band is expected to be present in the spectra of the FU-loaded samples. Nevertheless, the presence of PO_4^{3-} anions is manifested by the downshift of the main silicate band to 1012 cm^{-1} for the two FU-loaded CaT-Z samples (Fig. 5). Apparently, the PO_4^{3-} content of loaded NZ (FU-1) is not large enough to cause a clear shift of the 1019 cm^{-1} band. This is in line with the results in Table S1 where the P_2O_5 content increases from 0.16 wt% in loaded NZ (FU-1) to 0.93 wt% in CaT-Z (FU-1), the corresponding SiO_2 content being 67.7 and 67.1 wt%, respectively (average EPMA values from two measurements: #4-5 and #6-7). Additional evidence for the presence of PO_4^{3-} ions is provided by the shoulder at ca. 570 cm^{-1} observed in the spectra of the FU-loaded CaT-Z samples, attributed to $v_4(PO_4^{3-})$.

The appearance of the broad peak centered at ca. 1445 cm^{-1} in the spectra of the loaded NZ (FU-1) and CaT-Z (FU-1 and FU-2) samples (Fig. 5) can be assigned to the $v_4(NH_4^+)$ mode of tetrahedral ammonium ions, considering that the same mode is measured at 1400 cm^{-1} for NH_4Cl [40], while three bands at 1435, 1445 and 1470 cm^{-1} characterize struvite [38]. Naturally, the bending $v_4(NH_4^+)$ mode should be accompanied by the infrared active N—H stretching mode, $v_3(NH_4^+)$, of the ammonium ions. Indeed, inspection of the water/O—H stretching region in the inset of Fig. 5 shows the development of shoulders at ca. 2855 and 3070 cm^{-1} in the spectra of the loaded NZ and CaT-Z samples. These new features can be associated with N—H stretching, since the $v_3(NH_4^+)$ mode of NH_4Cl was reported at 3145 cm^{-1} [40]. Hydrogen bonding effects in the FU-loaded samples could be responsible for the observed downshift of $v_3(NH_4^+)$ to 2855 and 3070 cm^{-1}.

We note that the relatively low initial Mg^{2+} concentrations in FU-1 and FU-2 solutions, compared to the PO_4-P and NH_4-N ones (Table 1), resulted in low stoichiometric ratios of Mg:N:P. These suggest that struvite precipitation on the NZ and CaT-Z surface or in the liquid phase should occur to a limited extent. As the EDS spectra showed (Fig. S1D and E), a part of the Mg^{2+} ions was incorporated in the liquid phase precipitates. Thus, the desorption of NH_4–N from FU-1 loaded NZ and CaT-Z (as well as from FU-2 loaded CaT-Z) by using NaCl solution (see Section 3.5.3) suggests that the broad peak at 1445 cm^{-1} should be related mostly to ammonium ions adsorbed via ion exchange with zeolite cations [41] rather than to struvite precipitation.

3.1.5. BET analysis

The results of N_2 adsorption/desorption isotherms for NZ and CaT-Z (Supplementary material, Fig. S4) showed that the BET specific surface area, the total pore volume and the average pore diameter slightly increased from 32.37, 0.107 and 13.23 to 33.05 m^2/g, 0.120 cm^3/g and 14.54 nm for NZ and CaT, correspondingly. Both materials exhibited similar isotherm shapes. Based on the pore size classification, micro-, meso- and macropores are related in N_2 adsorption isotherm with relative pressures less than 0.1, 0.1–0.8 and 0.8–1.0P/P_0, respectively [42]. The average pore diameter and the distinct hysteresis loop observed at a relative pressure of about 0.4–0.8P/P_0 indicated the mesoporous (2–50 nm) structure of both NZ and CaT-Z [42].

3.2. Effect of contact time on P removal

3.2.1. Kinetic tests with FU-1 (NZ, CaT-Z)

When 50% FU-1 was treated with NZ (Fig. 6a). P concentration (C_t) started to decrease after the first 24 h reaching 97.4 mg/L in 96 h (R % = 48%) and then increased at 123.3 mg/L at 144 h (34.2%). This C_t

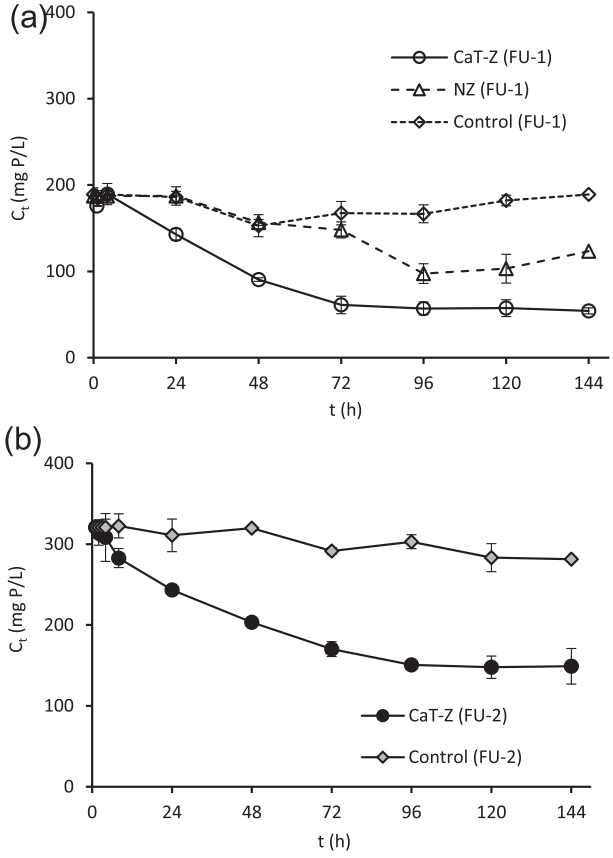

Fig. 6. Effect of contact time on P concentration (a) in 50% FU-1 in the presence and absence (control) of NZ and CaT-Z (C_0 = 189.5 mg P/L, adsorbent dosage = 10 g/L, initial pH = 5.8, T = 25 °C) and (b) in 50% FU-2 in the presence and absence (control) of CaT-Z (C_0 = 320.7 mg P/L, adsorbent dosage = 10 g/L, initial pH = 5.7, T = 25 °C).

fluctuation might be due to the desorption of loosely bound P from NZ surface. In the presence of CaT-Z, a precise decreasing trend of C_t in FU-1 was observed up to 144 h resulting in a lower residual P concentration (54.2 mg/L) (Fig. 6a) and higher removal (71.4%) than these with NZ. Removal of P from FU-1 reached an equilibrium in 72–96 h (69.9%). In contrast, P concentration in the control solution decreased from 186.2 to 152.9 mg/L between 24 and 48 h, and then increased at 189.0 mg P/L until 144 h. This behavior could be due to hydrolysis of polyphosphates into orthophosphates [43] or suspension of P precipitates in the liquid phase.

The final pH of 50% FU-1 after 144 h was found to increase from 5.80 (Table 1) to 7.53, 7.95 and 8.37 for the control, NZ and CaT-Z containing solutions, respectively. The pH increase at 7.53 in the control FU-1 was a result of urea hydrolysis (producing bicarbonate and ammonium ions) [16], while in the presence of NZ and CaT-Z, this increase was also attributed to the ionization of surface functional groups. The higher pH increase in the case of FU-1 with CaT-Z was attributed to the release of CO_3^{2-} groups from the CaT-Z surface into the solution (Fig. 5, Graphical Abstract). The chemical equations of the ligand exchange reaction are given in our previous work [28]. The urea hydrolysis and conversion to ammonium ions was indicated by the increase of NH_4-N concentration at values of 766, 1260 and 1928 mg/L in the control, NZ and CaT-Z solution, respectively.

3.2.2. Kinetic tests with FU-2 (CaT-Z)

In the mixture of 50% FU-2 with CaT-Z, C_t decreased to 149.1 mg/L (R% = 53.52%) at 144 h and P removal reached a plateau at 96 h (53.0%) (Fig. 6b). In the control solution, P concentration decreased only by 12% at 144 h (C_t = 281.4 mg/L). As also observed in FU-1, the

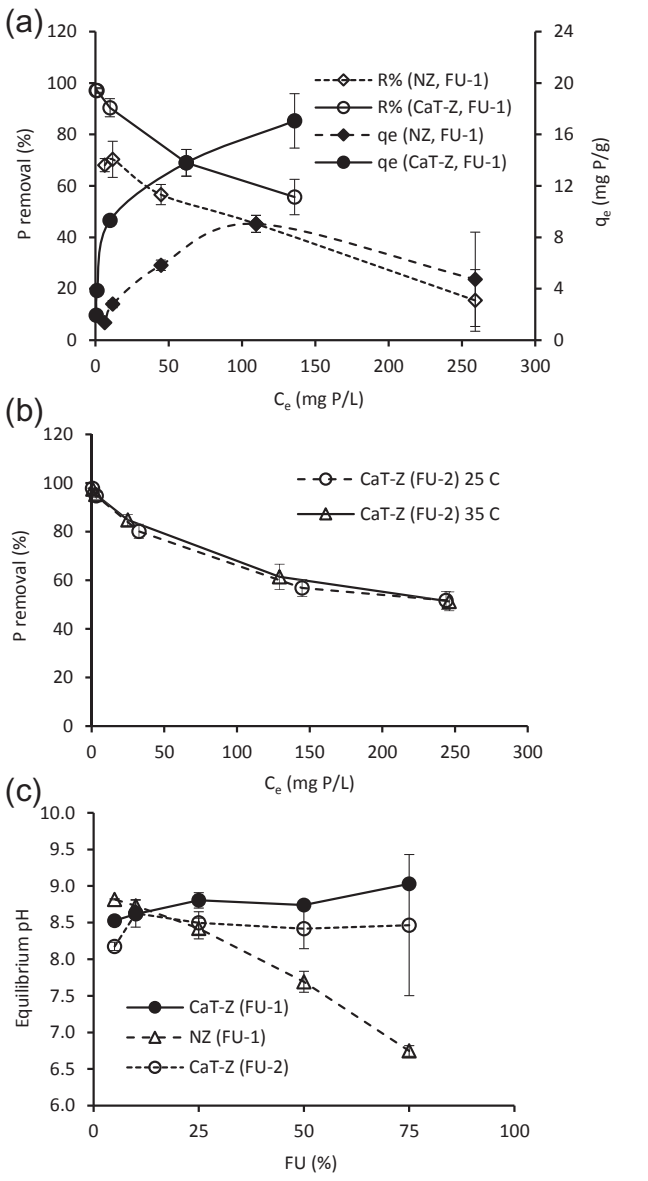

Fig. 7. Phosphorus removal efficiency (a) by NZ and CaT-Z in FU-1 at 25 °C, (b) by CaT-Z in FU-2 at 25 and 35 °C; (c) equilibrium pH at different FU-1 and FU-2 dilution ratios at 25 °C (adsorbent dosage = 10 g/L, contact time = 144 h, initial pH = 5.7 and 5.8 for FU-1 and FU-2, respectively). Note: the high SD (± 0.96) at the final pH (mean = 8.47) of 75% FU-2 in the presence of CaT-Z was due to the deviation of one pH value (7.35) compared to other two (9.05 and 9.00).

presence of CaT-Z in FU-2 resulted in a higher and faster reduction of P concentration. In the control solution of FU-2, the decrease of P concentration was due to the spontaneous P precipitation mainly with Ca^{2+} and in less extent with Mg^{2+} [16], because the initial Mg^{2+} concentration in FU-2 was much lower than these of Ca^{2+} (Table 1). Slow adsorption kinetics of P onto CaT-Z was also observed in aqueous solutions [28]. In contrast, phosphate removal from fresh synthetic human urine by hybrid anion exchange resin and Zr-based metal organic frameworks (MOFs) was completed within minutes [11,27].

3.3. Effect of FU-1 and FU-2 dilution on P removal

3.3.1. Effect of FU-1 dilution (NZ, CaT-Z)

Phosphorus removal by CaT-Z increased from 55.7% to 97.1% when the dilution ratio of FU-1 with DI increased from 25/75 (75% FU-1) to

95/5 (5% FU-1) (Fig. 7a). This resulted in residual P concentrations (C_e) of 0.58–135.82 mg/L after 144 h. In the presence of NZ, the *R%* increased from 15.5% to 70.3% in the range of 75% and 10% FU-1, and then slightly decreased to 68.1% in 5% FU-1. The C_e was found to be 6.39–259.02 mg/L (Fig. 7a). Therefore, CaT-Z exhibited higher P removal efficiencies and lower residual P concentrations in FU-1 than these of NZ.

The significant difference of P removal efficiency (15.5% and 45.2%) by NZ between the dilution ratios of 25/75 and 50/50 was attributed to the acidic equilibrium pH (6.75) in the 25/75 diluted FU-1 (Fig. 7c), which made unfavorable the liquid phase or surface precipitation of P as calcium phosphate [30]. In the case of FU-1 and FU-2 treated with CaT-Z, all equilibrium pH values were alkaline, namely in the range of 8.53–9.03 and 8.18–8.63, respectively (Fig. 7c). This suggests a more positive effect of CaT-Z on FU equilibrium pH due to the ligand exchange mechanism (Fig. 5).

3.3.2. Effect of FU-2 dilution (CaT-Z)

When FU-2 sample was treated with CaT-Z, the *R%* increased from 51.7% to 97.8% at 25 °C and from 51.3% to 97.4% at 35 °C with the increasing dilution ratio of FU-2 from 25/75 to 95/5 (Fig. 7b). Thus, the increase of FU-2 temperature from 25 to 35 °C did not significantly affect the *R%* at all studied urine dilution ratios. The range of *R%* values for CaT-Z in FU-2 were similar to these in FU-1. After 144 h, the C_e in FU-2 at 25 and 35 °C was found to be 0.66–243.79 and 0.76–245.93 mg/L, respectively (Fig. 7b). However, the effect of FU temperature on P adsorption/removal by CaT-Z should be further tested at lower and higher temperatures in order to simulate various climate conditions.

The high P removal efficiency (> 90.4%) of CaT-Z at the highest dilution ratios (90/10 and 95/5) of FU-1 and FU-2, which mean 10 and 20 times dilution, suggests a benefit of the adsorption process compared to the struvite precipitation method because the higher the urine dilution the lower the P removal by struvite crystallization [16]. This is important regarding the simplicity/flexibility of the adsorption technique under various FU dilution conditions and compositions since through source separation large amounts of undiluted or low diluted (2–10 times) urine can be collected depending on the flushing system [13,44]. In contrast, entering the sewage system, urine may be diluted up to 100 times [11].

3.3.3. Adsorption isotherms and comparison with other materials

The equilibrium data at different dilution ratios of FU-1 and FU-2 in the presence of CaT-Z fitted very well the isotherm model of Temkin (at 25 °C for FU-1) and Freundlich (at 25 and 35 °C for FU-2) suggesting P adsorption on heterogeneous surfaces (Supplementary material, Table S2). The linear form of isotherm models were evaluated based on the highest coefficient of determination (R^2) and the lowest root mean square error (*RMSE*), as described in our previous work [28]. The values of Freundlich constant n (> 1) indicated a favorable P adsorption. However, we note that the calculated model parameters were overestimated because P precipitation in the liquid phase significantly contributed to the total P removal overestimating thus the q_e values at all dilution ratios.

A comparison of the Langmuir maximum P adsorption capacity (q_m) of CaT-Z (Table S2) with q_m or q_e of other adsorbents used for P recovery from human urine is presented in Table 4. In order to avoid a comparison based only on the overestimated experimental q_e or q_m values, the total P desorption capacity (q_{des}) of loaded CaT-Z in 75% FU-1 (9.47 ± 1.20 mg/g) and 25% FU-2 (11.11 ± 1.05 mg/g), as estimated in Section 3.5, is given in Table 4 (see parentheses). It is obvious that CaT-Z exhibited a sufficient P adsorption capacity even taking into account the q_{des} values. Besides, the particle size range of CaT-Z allows an easier solid/liquid separation by sieving compared with the centrifugation needed for the natural loess or Zr-based MOF nanoparticles (Table 4). The soil-friendly loaded CaT-Z can be directly used as soil amendment without to be regenerated, providing slow-released nutrients and improving the soil water holding capacity and hydraulic conductivity [45]. Instead of that, exhausted HAIX resins are not recommended for soil incorporation and need caustic brine regeneration solution as well as Ca/Mg salts for P recovery, despite their faster and higher P removal efficiency (up to 97%) [11,25,26] (Table 4).

3.4. Effect of initial FU-2 pH on P removal

The P removal was not affected by the increase of initial pH of 50% FU-2 from 5 to 7 ranging between 67.3 and 68.8% (Fig. 8). This finding is important considering that real FU pH usually is around 6.0 [10,17], so pH adjustment is not required for FU treatment by CaT-Z. However, the *R%* decreased to 58% when the initial pH was adjusted to 8. As also observed in the kinetic and equilibrium tests, the final pH increased in all cases at 8.11–9.10 (Fig. 8) due to urea hydrolysis and ligand exchange mechanism. In the range of the examined initial and final pH of 50% FU-2, the CaT-Z surface was always positively charged because pH was lower than the surface point of zero charge ($pH_{pzc} \approx 9.90$), as determined by the drift method [28].

At initial FU-2 pH 5–7 and before it increased at values higher than 7.2 during adsorption, the dominant phosphate species was the monovalent $H_2PO_4^-$ ($pK_1 = 2.15$). When FU-2 pH continued to increase at values ≥ 7.2, the dominant species became the divalent HPO_4^{2-} ($pK_2 = 7.20$) [18,26] and the final pH approached the pH_{pzc}. So, at pH 8, CaT-Z surface contained less positively charged binding sites ($\equiv Ca-OH_2^+$) [28] which shifted to neutral ($\equiv Ca-OH$) at final pH [11,25]. At this pH, the electrostatic interactions between $\equiv Ca-OH_2^+$ and $H_2PO_4^-/HPO_4^{2-}$ were weaker and less outer-sphere surface complexes were formed [24]. The decrease of *R%* at pH 8 could also be due to the more negative impact of bicarbonate anions (produced during urea hydrolysis) in the early stage of adsorption which compete with phosphate for the formation of Ca complexes [16].

3.5. Desorption studies

3.5.1. Fractionation of P from FU-1 loaded NZ and CaT-Z

The sequential extraction method applied to the FU-1 loaded CaT-Z showed that the increasing dilution of FU-1 from 75% to 5% FU-1 led to the percentage decrease of the Ca and Mg associated P (denoted as Ca + Mg-P or HCl-P) from 47% to 13.1% of the total removed P (*R%*) and to the increase of the loosely bound P (LB-P or $NaHCO_3$-P) from 6.7% to 58.6% (Fig. 9a) [32]. At the lowest diluted FU-1 (75% and 50% FU-1) the dominant P species on CaT-Z was found to be the Ca + Mg-P (47% and 64.8% of *R%*, respectively) (Fig. 9a). On the other hand, at the highest diluted FU-1 (10% and 5% FU-1) the dominant P fraction on CaT-Z was the LB-P with 26.3% and 58.6%, respectively.

An opposite trend for the Ca + Mg-P fraction was observed for the FU-1 loaded NZ (Fig. 9a), since it increased from 0.8% to 39.7% of *R%* with increasing FU-1 dilution from 75% to 5% FU-1 indicating that more Ca + Mg-P precipitates were trapped from the liquid phase onto NZ surface at higher FU-1 dilution ratios. This finding should be unexpected regarding the higher Ca^{2+} and Mg^{2+} concentrations in less diluted FU-1 which favor the Ca-P and Mg-P precipitation. However, it can be explained by the slightly acidic (6.75) and alkaline (7.69) final pH in 75% and 50% FU-1, respectively (Fig. 7c), which made the formation of Ca-P or Mg-P nuclei/complexes in the liquid phase impossible or less favorable [31,46]. The LB-P on NZ increased from 2.1% to 11.2% of *R%* at 75% and 5% FU-1, respectively. The P fraction bound to aluminum (hydro)oxides of NZ (Al-P or NaOH-P) [32] raised from 3.4% to 21.7% of *R%* with increasing FU-1 dilution. These values were higher than these of the FU-1 loaded CaT-Z (1.8–13.2%). The Al-P form contributed more on *R%* than LB-P in 5% and 10% FU-1 loaded NZ (Fig. 9a).

In the case of FU-1 loaded NZ, the total P desorption efficiency (*D%*) of the three extraction steps corresponded to 6.2%, 22.4%, 41.7% and 72.6% of the total removed P from 75%, 50%, 10% and 5% FU-1,

Table 4
Comparison of phosphate P adsorption capacity from human urine by various adsorbents and resins.

Adsorbent	Particle diameter (mm)	Urine type[a]	q_e or q_m (mg P/g)	Reference
CaT-Z	0.5–1.19	Real FU (FU-1)	15.54 (9.47)[b]	This study
CaT-Z	0.5–1.19	Real FU (FU-2)	15.14 (11.11)[b]	This study
Natural loess	< 0.075	Real HU	4.01	[24]
Hybrid anion exchange resin with hydrous ferric oxide (HAIX-Fe)[c]	–	Synthetic FU	10.2	[25]
Hybrid anion exchange resin with hydrous ferric oxide (HAIX-Fe)	–	Synthetic FU	10.1	[26]
		Synthetic HU	6.9	
Hybrid anion exchange resin impregnated with hydrous ferric oxide nanoparticles	0.3–1.2	Synthetic FU	10.1	[11]
		Synthetic HU	5.35	
Zr-based metal organic framework (UiO-66)	200–500 nm	Synthetic FU	224.70	[27]
Zr-based metal organic framework plus NH_2 (UiO-66-NH2)	200–500 nm	Synthetic FU	292.57	[27]

[a] FU: fresh urine; HU: hydrolyzed urine.
[b] Values in parentheses correspond to the total P desorption capacity, q_{des} (mg/g), of loaded CaT-Z in 75% FU-1 and 25% FU-2 as calculated by a three-step desorption procedure in Section 3.5.
[c] Column study.

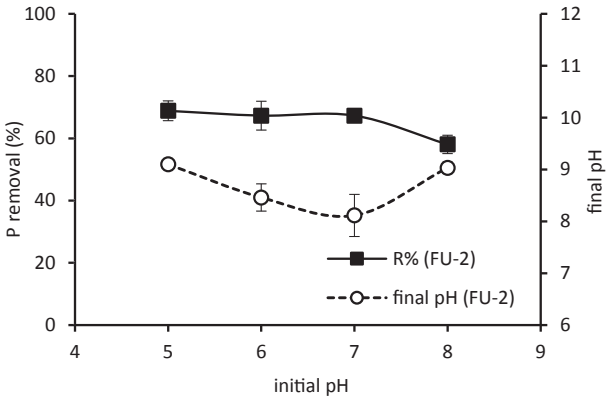

Fig. 8. Effect of initial FU-2 pH on P removal efficiency in the presence of CaT-Z (C_0 = 394.8 mg P/L, adsorbent dosage = 10 g/L, contact time = 144 h, T = 25 °C).

respectively (sum of 3 steps in Fig. 9a). The respective P desorbed from the FU-1 loaded CaT-Z was 55.5%, 75.6%, 55.1% and 84.9% of the total *R%*. Therefore, CaT-Z provided higher P desorption capacities (q_{des}) along with lower P residual concentrations (C_e) than NZ at all dilution ratios of FU-1 (Table 5). Namely, the applied sequential desorption procedure demonstrated that a higher percentage of total removed P was recovered from loaded CaT-Z than from NZ. Furthermore, in 75%, 50% and 10% FU-1 treated with NZ, P was mainly removed in the liquid phase (*D%* less than 41.7% of *R%*) and outside the NZ surface due to precipitation with Ca and Mg ions. This shows that in the equilibrium tests with FU-1 at 25 °C, the q_e values of NZ were overestimated more than these of CaT-Z at all dilution ratios of FU-1. In contrast, the majority of the total removed P was recovered from the FU-1 loaded CaT-Z (*D%* > 55.1% of *R%*), indicating that the contribution of P adsorption on the total P removal was higher than that of the liquid phase precipitation at the studied FU-1 dilution ratios.

3.5.2. Fractionation of P from FU-2 loaded CaT-Z

The sequential desorption of P from the loaded CaT-Z in 25% FU-2 showed that the major fraction was the Ca + Mg-P (*D%* = 65.4%) followed by the LB-P (15.4%) (Fig. 9b). In 5% FU-2, the dominant fraction was the LB-P (50.6%) followed by the Ca + Mg-P (22.3%). The Al-P fraction was found to be very low at both dilution ratios (4.2% and 1.1%). The total amount of P desorbed from the 25% and 5% FU-2 loaded CaT-Z at the three steps was 84.9% and 74.1% of the total removed P (Fig. 9b) corresponding to a total q_{des} of 11.11 ± 1.05 and 2.13 ± 0.07 mg P/g, respectively (Table 4). The values of total P desorption efficiency (≥74.1% of *R%*) indicated again, as in FU-1, the low contribution of the liquid phase P precipitation to the total P removal when the CaT-Z was employed as adsorbent. The values of total q_{des} and these of *D%* of Ca + Mg-P and LB-P for the 25% and 5% FU-2 loaded CaT-Z present a similar trend to these of 50%, 10% or 5% FU-1 loaded CaT-Z which can be due to a similar magnitude of initial P concentration (Table 2).

3.5.3. Desorption of NH_4-N from FU-1 and FU-2 loaded adsorbents

The q_{des} of the loaded NZ for NH_4-N was found to be 5.81 ± 0.23, 5.93 ± 0.68, 5.55 ± 0.62 and 3.78 ± 0.24 mg N/g in 5%, 10%, 50% and 75% FU-1, respectively (Fig. 9c). For the FU-1 loaded CaT-Z, the corresponding values were 1.84 ± 0.24, 3.95 ± 0.32, 6.31 ± 0.24 and 6.09 ± 0.58 mg N/g. The q_{des} of the loaded CaT-Z in 5% and 50% FU-2 was 1.17 ± 0.14 and 3.02 ± 0.44 mg N/g, respectively. These results indicated that ammonium nitrogen was adsorbed onto NZ and CaT-Z through ion-exchange with zeolite external surface and framework cations [31,46]. The adsorption capacity and desorption efficiency (%) for NH_4-N could not be estimated due to the increasing NH_4-N concentration in FU-1 and FU-2 as a result of the continuing urea hydrolysis during the adsorption process.

3.6. Removal mechanisms of P

The experimental results showed that the total P removal from FU-1 and FU-2 was attributed to the following main processes: (i) precipitation in the liquid phase and (ii) adsorption on NZ or CaT-Z (removal in the solid phase) (Table 6). The liquid phase precipitation of P was confirmed by the EDS detection of Ca-P and Ca + Mg-P phases on the precipitates collected after the FU-1 treatment with NZ or CaT-Z (Table 3, Fig. S1). No Si^{4+} or Al^{3+} cations were detected in these particles distinguishing them clearly from the mineral adsorbents. The P removal in the liquid phase was also indicated by the sequential desorption procedure applied on the loaded NZ and CaT-Z because the total desorbed P (*D%*) of the three extraction steps was found to be lower than the total removed P (*R%*) calculated from the residual P concentration in FU-1 and FU-2 (Fig. 9a and b). Although we macroscopically estimated a very low amount of P containing precipitates, their collection from the liquid phase after CaT-Z sieving can enhance the total P recovery of the process.

Regarding the P removal in the solid phase, three adsorption mechanisms [18] were indicated by the spectroscopic techniques and desorption studies (Table 6): i) inner-sphere surface complexation through ligand exchange, ii) surface precipitation of Ca-P complexes, and iii) outer-sphere surface complexation through electrostatic attraction. A schematic presentation of P adsorption mechanisms onto CaT-Z is given in Graphical Abstract. As we explain below, these mechanisms also occurred on NZ but to a less extent and in a different manner. In general, P accommodation on NZ and CaT-Z was confirmed by the SEM-EDS (Fig. S1), and verified more analytically by EPMA

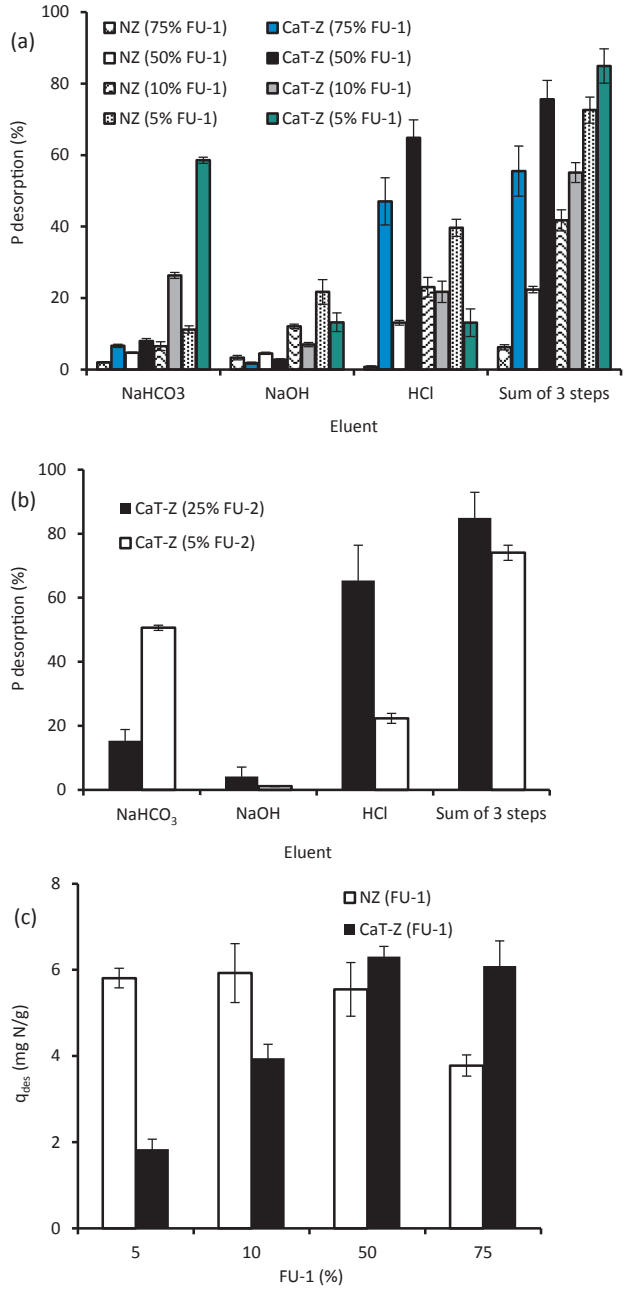

Fig. 9. Sequential desorption of P (a) from the loaded NZ and CaT-Z in 75%, 50%, 10% and 5% FU-1 and (b) from the loaded CaT-Z in 25% and 5% FU-2; (c) NH_4-N desorption capacity of the loaded NZ and CaT-Z in 75%, 50%, 10% and 5% FU-1 by using 1 M NaCl (adsorbent/eluent ratio = 10 g/L, contact time of each step = 24 h, T = 25 °C).

investigation revealing the spatial distribution of Ca-P phases and the correlation of Ca and P content on the adsorbents (Fig. 4, Fig. S2, Table S1).

The disappearance of the carbonate bands/features from the IR spectra of FU-1 and FU-2 loaded CaT-Z indicated the ligand exchange between the CO_3^{2-} groups (≡Ca−CO_3) of CaT-Z surface and phosphate anions ($H_2PO_4^-$ or HPO_4^{2-}) of FU-1 and FU-2 (Fig. 5). This specific adsorption mechanism did not occur in the presence of NZ in FU-1 and suggested the formation of a strong, covalent bond (Ca-O-P) between phosphate and Ca^{2+} ions at CaT-Z surface [18]. This stable Ca-P fraction could be extracted only by HCl (Fig. 9a and b, Table 6). So, CaT-Z worked as a ligand exchanger exhibiting a high selectivity for P even in diluted FU (Fig. 9a and b) and in the presence of competing FU anions (Cl^-, SO_4^{2-}, HCO_3^-). The mechanism of ligand exchange has been also confirmed earlier [28,29,36]. Depending on the phosphate ionic form in FU, the ligand exchange reaction can lead to the formation of four different inner-sphere surface complexes, described by corresponding chemical equations [24,28,42]. The monovalent $H_2PO_4^-$ and divalent HPO_4^{2-} anion can form the monodentate complexes (≡Ca−O)PO$(OH)_2$ and (≡Ca−O)PO_2(OH)], respectively, whereas HPO_4^{2-} can also form the bidentate mononuclear (≡Ca−O_2)PO(OH) or bidentate binuclear complex (≡Ca−$O)_2$PO(OH).

A different inner-sphere complexation of phosphate with Al-OH surface groups [33] was indicated by the NaOH extractable P (Table 6) and the bulk detection of berlinite mineral ($AlPO_4$) in the XRD spectra of loaded NZ and CaT-Z in 50% FU-1 and FU-2, respectively (Fig. S3). According to the desorption data, the non-labile Al-P fraction [33] was more important for NZ than for CaT-Z (Fig. 9a) but in general was minor compared with Ca + Mg-P because *D%* of NaOH-P was up to 21.7% and 4.2% of the total *R%* in FU-1 and FU-2, respectively (Fig. 9a and b).

Micrographs and in-situ elemental analyses of SEM-EDS and EPMA revealed the presence of Ca-P or apatite microcrystals on clinoptilolite mineral in loaded NZ and CaT-Z (Fig. S1C) or on the plagioclase in NZ (Fig. 2). These findings indicate the mechanism of surface precipitation (Table 6) which can be related to a multilayer adsorption of Ca + Mg-P fraction [28]. Surface precipitation can be resulted as continuation of surface complexation [28,47] or even from the oversaturation of the precipitate constituents (Ca and phosphate) in a finite solution volume surrounding the adsorbent surface [18]. In the case of NZ, the higher desorption efficiency of Ca + Mg-P (23.1% and 39.7% of *R%*) was observed in 10% and 5% FU-1 that should be attributed to the ammonium adsorption (Fig. 9c) through ion exchange and the release of Ca^{2+} ions from zeolite into the solution [30]. After that and under alkaline pH conditions (Fig. 7c), Ca^{2+} and phosphate ions could be co-precipitated onto NZ surface or in the liquid phase outside the adsorbent [18,30,31].

The sequential desorption procedure revealed that urine dilution, namely initial P concentration, affected the fractionation of adsorbed P which corresponds to definite adsorption mechanisms. To our knowledge, the effect of FU dilution on adsorbed P speciation has not been extensively studied in the literature [17,24,26]. In less diluted urine (75% and 50% FU-1 or 25% FU-2), P was mainly adsorbed on CaT-Z via the non-labile Ca + Mg-P form (HCl-P) (Fig. 9a and b) suggesting as

Table 5
Total P desorption capacity (q_{des}) of NZ and CaT-Z at different dilution ratios of FU-1.

Dilution ratio (V_{DI}/V_{urine})	%FU	C_o (mg P/L)*	C_e (mg P/L)		q_{des} (mg P/g)	
			NZ	CaT-Z	NZ	CaT-Z
25/75	75	306.39 ± 7.87	259.02 ± 36.70	135.82 ± 21.13	0.30 ± 0.03	9.47 ± 1.20
50/50	50	199.99 ± 4.18	109.52 ± 6.61	62.03 ± 10.37	2.02 ± 0.08	10.43 ± 0.73
90/10	10	39.89 ± 3.44	11.83 ± 2.80	1.16 ± 0.27	1.17 ± 0.08	2.13 ± 0.11
95/5	5	20.02 ± 0.31	6.39 ± 0.51	0.58 ± 0.21	0.99 ± 0.05	1.65 ± 0.09

* The values of C_O, taken from Table 2, are given here with two decimals for better comparison with C_e and q_{des}.

Table 6
Proposed removal mechanisms of P from FU-1 and FU-2 as indicated by various analytical techniques and experimental procedures.

Removal mechanism	Analytical technique/experimental procedure	Indication	Adsorbent
Inner-sphere complexation (adsorption)	XRD	Berlinite (Al-P)	NZ, CaT-Z
	IR-ATR	Disappearance of carbonate bands/features (ligand exchange with phosphate)	CaT-Z
	Desorption	HCl-P extraction (Ca + Mg-P)*	CaT-Z
	Desorption	NaOH-P extraction (Al-P)	NZ, CaT-Z
Outer-sphere complexation (adsorption)	Desorption	$NaHCO_3$–P extraction (LB-P)	NZ, CaT-Z
Surface precipitation (adsorption)	SEM-EDS	Ca-P precipitates on clinoptilolite	NZ, CaT-Z
	EPMA	Ca-P crystals on plagioclase	NZ
	Desorption	HCl-P extraction (Ca + Mg-P)*	NZ, CaT-Z
Liquid phase precipitation	SEM-EDS	Ca-P and Ca + Mg-P precipitates	NZ, CaT-Z
	Desorption	Total *D%* lower than total *R%*	NZ, CaT-Z

* The Ca + Mg-P fraction (HCl-P) mainly corresponds to a Ca-P form because the initial Mg concentrations in FU-1 and FU-2 were much lower than these of Ca^{2+} (see Table 1).

dominant adsorption mechanism the inner-sphere complexation (ligand exchange). A part of the Ca + Mg-P was adsorbed through surface precipitation (Graphical Abstract, Fig. S1C). In more diluted urine (10% and 5% FU-1 or 5% FU-2), the loosely bound P ($NaHCO_3$-P) was the major adsorbed fraction on CaT-Z followed by the Ca + Mg-P (due to ligand exchange), suggesting the dominant role of outer-sphere complexation via electrostatic attraction (Table 6, Graphical Abstract) [18]. In this very fast, non-specific, reversible and physical adsorption process, the inner hydration shell of the adsorbate is retained, namely water molecules are located between the adsorbent and the adsorbed phosphate [18]. The outer-sphere complexation (LB-P) did not play a significant role in NZ (Fig. 9a) due to its low pH_{pzc} (6.54) compared with that of CaT-Z (9.90).

Concluding, CaT-Z adsorbed more P than NZ (Table 5) due to the dominant contribution of ligand exchange mechanism to P adsorption in less diluted FU, and due to the enhanced outer-sphere complexation in more diluted FU. The lower P removal and adsorption by NZ was a result of weaker electrostatic attraction and minor surface precipitation of Ca-P complexes formed in the liquid phase [31]. The speciation of adsorbed P plays an important role regarding its plant availability in case of using the FU loaded CaT-Z as soil amendment. The Ca + Mg-P and Al-P fractions are considered as poorly labile under natural water conditions (pH 5–9) [32], whereas the $NaHCO_3$ extractable P (Olsen-P) represents the plant available and easily water soluble fraction [48]. The evaluation of fertilization efficiency of urine loaded CaT-Z in pot or field trials and the techno-economic assessment of a full-scale FU treatment by CaT-Z are interesting issues for further studies. However, they are out of the purpose of this lab-scale research.

4. Conclusions

Natural clinoptilolite treated with $Ca(OH)_2$ exhibited an enhanced P adsorption and removal from real fresh urine compared with the raw material. Phosphorus adsorption onto CaT-Z was efficient at original FU pH without adjustment and in two different FU samples. Bulk and in-situ analytical techniques suggested that P adsorption on both NZ and CaT-Z was a complex process involving various mechanisms. The sequential P desorption from the loaded adsorbents further demonstrated these mechanisms, revealed the influence of FU dilution (initial P concentration) on adsorbed P speciation, and confirmed that more P adsorbed onto CaT-Z surface than precipitated in the liquid phase at all FU dilution ratios. A total desorption capacity of 10.43 and 11.11 mg P/g was found for FU-1 and FU-2 loaded CaT-Z, respectively. Ligand exchange was the dominant P adsorption mechanism on CaT-Z in less diluted urine, whereas outer-sphere complexation accompanied by ligand exchange was the major one in more diluted FU. Desorption tests with NaCl and IR-ATR spectra indicated that besides P, NZ and CaT-Z adsorbed ammonium nitrogen.

The results of this research suggested the efficient use of CaT-Z for phosphate recovery from real human urine. As an important, primary point source of phosphate, urine can be treated with the low-cost and eco-friendly CaT-Z to reduce phosphate discharges in the environment and to recover an essential and non-renewable nutrient for agricultural applications. Further studies should be conducted to investigate the contamination of fresh urine loaded CaT-Z with pathogens and pharmaceutical residues, and the behaviour of CaT-Z as simultaneous P and N adsorbent in hydrolysed urine.

Acknowledgements

This research did not receive any specific grant from funding agencies in the public, commercial, or not-for-profit sectors. We would like to thank the anonymous reviewers for their critical comments that improved the manuscript.

Appendix A. Supplementary data

Supplementary data associated with this article can be found, in the online version, at http://dx.doi.org/10.1016/j.cej.2018.04.102.

References

[1] R. Kumar, P. Pal, Assessing the feasibility of N and P recovery by struvite precipitation from nutrient-rich wastewater: a review, Environ. Sci. Pollut. Res 22 (2015) 17453–17464.
[2] J.A. Wilsenach, C.A.H. Schuurbiers, M.C.M. van Loosdrecht, Phosphate and potassium recovery from source separated urine through struvite precipitation, Water Res. 41 (2007) 458–466.
[3] S.G. Barbosa, L. Peixoto, B. Meulman, M.M. Alves, M.A. Pereira, A design of experiments to assess phosphorous removal and crystal properties in struvite precipitation of source separated urine using different Mg sources, Chem. Eng. J. 298 (2016) 146–153.
[4] D.P. Van Vuuren, A.F. Bouwman, A.H.W. Beusen, Phosphorus demand for the 1970–2100 period: a scenario analysis of resource depletion, Global Environ. Change 20 (2010) 428–439.
[5] H. Heinonen-Tanski, A. Sjöblom, H. Fabritius, P. Karinen, Pure human urine is a good fertiliser for cucumbers, Bioresour. Technol. 98 (2007) 214–217.
[6] Z.S. Ban, G. Dave, Laboratory studies on recovery of N and P from human urine through struvite crystallisation and zeolite adsorption, Environ. Technol. 25 (2004) 111–121.
[7] T. Karak, P. Bhattacharyya, Human urine as a source of alternative natural fertilizer in agriculture: a flight of fancy or an achievable reality, Resour. Conserv. Recycl. 55 (2011) 400–408.
[8] B. Etter, E. Tilley, R. Khadka, K.M. Udert, Low-cost struvite production using source-separated urine in Nepal, Water Res. 45 (2011) 852–862.
[9] S. Zhang, C.Y. Lim, C.-L. Chen, H. Liu, J.-Y. Wang, Urban nutrient recovery from fresh human urine through cultivation of *Chlorella sorokiniana*, J. Environ. Manage. 145 (2014) 129–136.
[10] B.-B. Lind, Z. Ban, S. Bydén, Nutrient recovery from human urine by struvite crystallization with ammonia adsorption on zeolite and wollastonite, Bioresour.

Technol. 73 (2000) 169–174.
[11] A. Sendrowski, T.H. Boyer, Phosphate removal from urine using hybrid anion exchange resin, Desalination 322 (2013) 104–112.
[12] Y. Chang, Z. Wu, L. Bian, D. Feng, D.Y.C. Leung, Cultivation of *Spirulina platensis* for biomass production and nutrient removal from synthetic human urine, Appl. Energy 102 (2013) 427–431.
[13] S.K. Pradhan, A. Mikola, R. Vahala, Nitrogen and phosphorus harvesting from human urine using a stripping, absorption, and precipitation process, Environ. Sci. Technol. 51 (2017) 5165–5171.
[14] M. Maurer, W. Pronk, T.A. Larsen, Treatment processes for source-separated urine, Water Res. 40 (2006) 3151–3166.
[15] S. Dutta, B. Vinnerås, Fertilizer from dried human urine added to ash and lime–a potential product from eco-sanitation system, Water Sci. Technol. 74 (2016) 1436–1445.
[16] X. Liu, G. Wen, H. Wang, X. Zhu, Z. Hu, Fate of phosphorus in diluted urine with tap water, Chemosphere 113 (2014) 146–150.
[17] N.P. Kocatürk, B.B. Baykal, Recovery of plant nutrients from dilute solutions of human urine and preliminary investigations on pot trials, Clean – Soil Air Water 40 (2012) 538–544.
[18] P. Loganathan, S. Vigneswaran, J. Kandasamy, N.S. Bolan, Removal and recovery of phosphate from water using sorption, Crit. Rev. Env. Sci. Technol. 44 (2014) 847–907.
[19] N.Y. Acelas, B.D. Martin, D. López, B. Jefferson, Selective removal of phosphate from wastewater using hydrated metal oxides dispersed within anionic exchange media, Chemosphere 119 (2015) 1353–1360.
[20] B. Beler-Baykal, A.D. Allar, S. Bayram, Nitrogen recovery from source-separated human urine using clinoptilolite and preliminary results of its use as fertilizer, Water Sci. Technol. 63 (2011) 811–817.
[21] B.B. Baykal, N. Kocaturk, A. Allar, B. Sari, The effect of initial loading on the removal of ammonium and potassium from source-separated human urine via clinoptilolite, Water Sci. Technol. 60 (2009) 2515–2520.
[22] S. Xu, L. Luo, H. He, H. Liu, L. Cui, Nitrogen and phosphate recovery from source-separated urine by dosing with magnesite and zeolite, Pol. J. Environ. Stud. 24 (2015) 2269–2275.
[23] Z. Ganrot, G. Dave, E. Nilsson, Recovery of N and P from human urine by freezing, struvite precipitation and adsorption to zeolite and active carbon, Bioresour. Technol. 98 (2007) 3112–3121.
[24] S. Jiang, X. Wang, S. Yang, H. Shi, Characteristics of simultaneous ammonium and phosphate adsorption from hydrolysis urine onto natural loess, Environ. Sci. Pollut. Res. 23 (2016) 2628–2639.
[25] J.A. O'Neal, T.H. Boyer, Phosphorus recovery from urine and anaerobic digester filtrate: comparison of adsorption-precipitation with direct precipitation, Environ. Sci. Water Res. Technol. 1 (2015) 481–492.
[26] J.A. O'Neal, T.H. Boyer, Phosphate recovery using hybrid anion exchange: applications to source-separated urine and combined wastewater streams, Water Res. 47 (2013) 5003–5017.
[27] K.-Y.A. Lin, S.-Y. Chen, A.P. Jochems, Zirconium-based metal organic frameworks: highly selective adsorbents for removal of phosphate from water and urine, Mater. Chem. Phys. 160 (2015) 168–176.
[28] D. Mitrogiannis, M. Psychoyou, I. Baziotis, V.J. Inglezakis, N. Koukouzas, N. Tsoukalas, D. Palles, E. Kamitsos, G. Oikonomou, G. Markou, Removal of phosphate from aqueous solutions by adsorption onto $Ca(OH)_2$ treated natural clinoptilolite, Chem. Eng. J. 320 (2017) 510–522.
[29] G. Markou, D. Mitrogiannis, V. Inglezakis, K. Muylaert, N. Koukouzas, N. Tsoukalas, E. Kamitsos, D. Palles, I. Baziotis, Ca(OH)2 pre-treated bentonite for phosphorus removal and recovery from synthetic and real wastewater, Clean Soil Air Water 46 (2018) 1700378-n/a.
[30] C. Wan, S. Ding, C. Zhang, X. Tan, W. Zou, X. Liu, X. Yang, Simultaneous recovery of nitrogen and phosphorus from sludge fermentation liquid by zeolite adsorption: mechanism and application, Sep. Purif. Technol. 180 (2017) 1–12.
[31] L. Lin, C. Wan, D.-J. Lee, Z. Lei, X. Liu, Ammonium assists orthophosphate removal from high-strength wastewaters by natural zeolite, Sep. Purif. Technol. 133 (2014) 351–356.
[32] C. Han, Z. Wang, W. Yang, Q. Wu, H. Yang, X. Xue, Effects of pH on phosphorus removal capacities of basic oxygen furnace slag, Ecol. Eng. 89 (2016) 1–6.
[33] D. Guaya, M. Hermassi, C. Valderrama, A. Farran, J.L. Cortina, Recovery of ammonium and phosphate from treated urban wastewater by using potassium clinoptilolite impregnated hydrated metal oxides as N-P-K fertilizer, J. Environ. Chem. Eng. 4 (2016) 3519–3526.
[34] M. Zhang, H. Zhang, D. Xu, L. Han, D. Niu, B. Tian, J. Zhang, L. Zhang, W. Wu, Removal of ammonium from aqueous solutions using zeolite synthesized from fly ash by a fusion method, Desalination 271 (2011) 111–121.
[35] APHA, Standard Methods for the Examination of Water and Wastewater, American Public Health Association, American Water Works Association, Water Environment Federation, Washington DC, 1999.
[36] G. Markou, V.J. Inglezakis, D. Mitrogiannis, I. Efthimiopoulos, M. Psychoyou, P. Koutsovitis, K. Muylaert, I. Baziotis, Sorption mechanism(s) of orthophosphate onto $Ca(OH)_2$ pretreated bentonite, RSC Adv. 6 (2016) 22295–22305.
[37] D. Palles, I. Konidakis, C. Varsamis, E. Kamitsos, Vibrational spectroscopic and bond valence study of structure and bonding in Al_2O_3-containing AgI–$AgPO_3$ glasses, RSC Adv. 6 (2016) 16697–16710.
[38] V. Stefov, B. Šoptrajanov, I. Kuzmanovski, H. Lutz, B. Engelen, Infrared and Raman spectra of magnesium ammonium phosphate hexahydrate (struvite) and its isomorphous analogues. III. Spectra of protiated and partially deuterated magnesium ammonium phosphate hexahydrate, J. Mol. Struct. 752 (2005) 60–67.
[39] C.-P.E. Varsamis, E.I. Kamitsos, T. Minami, N. Machida, Investigation of CuI-containing molybdophosphate glasses by infrared reflectance spectroscopy, J. Phys. Chem. C 116 (2012) 11671–11681.
[40] K. Nakamoto, Chapter 2, Applications in Inorganic Chemistry, Infrared and Raman Spectra of Inorganic and Coordination Compounds, Part A, J. Wiley & Sons, New York, 1978, p. 135.
[41] I. Rodríguez-Iznaga, G. Rodríguez-Fuentes, A. Benítez-Aguilar, The role of carbonate ions in the ion-exchange $Ni^{2+} = 2NH_4^+$ in natural clinoptilolite, Microporous Mesoporous Mater. 41 (2000) 129–136.
[42] J. Lin, Z. Zhang, Y. Zhan, Effect of humic acid preloading on phosphate adsorption onto zirconium-modified zeolite, Environ. Sci. Pollut. Res 24 (2017) 12195–12211.
[43] P. Jin, W. Ren, C. Liang, X. Wang, L. Zhang, The study on the separate collection and nutrients recovery of urine in municipal wastewater, Desalin. Water Treat. 52 (2014) 5031–5036.
[44] S. Başakçilardan-Kabakci, A.N. İpekoğlu, I. Talinli, Recovery of ammonia from human urine by stripping and absorption, Environ. Eng. Sci. 24 (2007) 615–624.
[45] D. Guaya, C. Valderrama, A. Farran, T. Sauras, J.L. Cortina, Valorisation of N and P from waste water by using natural reactive hybrid sorbents: nutrients (N, P, K) release evaluation in amended soils by dynamic experiments, Sci. Total Environ. 612 (2018) 728–738.
[46] H. Huang, D. Xiao, R. Pang, C. Han, L. Ding, Simultaneous removal of nutrients from simulated swine wastewater by adsorption of modified zeolite combined with struvite crystallization, Chem. Eng. J. 256 (2014) 431–438.
[47] I. Perassi, L. Borgnino, Adsorption and surface precipitation of phosphate onto $CaCO_3$–montmorillonite: effect of pH, ionic strength and competition with humic acid, Geoderma 232–234 (2014) 600–608.
[48] M. Yang, J. Lin, Y. Zhan, Z. Zhu, H. Zhang, Immobilization of phosphorus from water and sediment using zirconium-modified zeolites, Environ. Sci. Pollut. Res 22 (2015) 3606–3619.